

## Research Article

<https://doi.org/10.1631/jzus.A2200198>



# Experimental and numerical study of seepage-induced suffusion under $K_0$ stress state

Tuo WANG<sup>1,2</sup>, Feng-shou ZHANG<sup>1,2✉</sup>, Pei WANG<sup>3</sup>

<sup>1</sup>Key Laboratory of Geotechnical & Underground Engineering of Ministry of Education, Tongji University, Shanghai 200092, China

<sup>2</sup>Department of Geotechnical Engineering, College of Civil Engineering, Tongji University, Shanghai 200092, China

<sup>3</sup>Department of Civil and Environmental Engineering, The Hong Kong Polytechnic University, Kowloon, Hong Kong 999077, China

**Abstract:** Suffusion in gap-graded soil involves selective erosion of fine particles through the pores formed by coarse particles under seepage forces. As the fines content (FC) decreases, the hydraulic and mechanical behavior of the soil will change, posing a huge threat to engineering safety. In this study, we first conduct a series of experimental tests of suffusion by using gap-graded soils and then analyze the evolution process of suffusion and the effect of the hydraulic gradient. Subsequently, according to the physical model, a discrete element method (DEM) numerical model with dynamic fluid mesh (DFM) is developed to extend the experimental study to the pore scale. Our results reveal the migration process of fines and the formation of erosion zones. A parametric study is then conducted to investigate the effect of the hydraulic gradient, FC, and  $K_0$  pressure (which limits the lateral displacement of the sample and applies vertical pressure) on eroded weight. The results show that the eroded weight increases with the increase of the hydraulic gradient and FC but decreases with the increase of  $K_0$  pressure.

**Key words:** Suffusion; Gap-graded soil; Discrete element method (DEM); Dynamic fluid mesh (DFM)


## 1 Introduction

Compared with continuously graded soils, fine particles in gap-graded and widely-graded soils are vulnerable to movement and loss under seepage force without damaging soil structures. The phenomenon is called suffusion (Chang and Zhang, 2011; Ke and Takahashi, 2014; Ji et al., 2017; Hu et al., 2019). Suffusion can deteriorate the soil strength and affect the stability of geotechnical engineering projects (Golay and Bonelli, 2011; Moffat et al., 2011; Luo et al., 2013; Tao et al., 2018; Wen et al., 2021; Yin et al., 2021). In addition, the process is challenging to monitor when not exposed at the surface, which makes it difficult to fully understand its evolution mechanism. According to statistics (Bendahmane et al., 2008), soil instability

caused by suffusion is one of the biggest threats to building structures, dams, and foundations (Wan and Fell, 2008; Yang et al., 2019).

The potential for suffusion in soil samples mainly depends on the soil structure (internal factor) and occurrence state (external factor). Soil structure includes particle size (Liu et al., 2019), gradation (Shire et al., 2014), and particle shape (Tang et al., 2020; Wang et al., 2022a). External factors include the hydraulic gradient and the stress state (Moffat and Fannin, 2011). In the study of soil structure, Kenney and Lau (1985) developed filter rules based on the particle gradation curve, to assess whether soils are internally unstable and the effectiveness of that method has been demonstrated in numerous studies (Wan and Fell, 2008; Chang and Zhang, 2011; Hunter and Bowman, 2018; Jin et al., 2021). Hu et al. (2019) conducted a series of numerical experiments to study the suffusion process of gap-graded and well-graded soils. Their results showed that under a large hydraulic gradient, the fines loss in well-graded soils was much lower than that in gap-graded soils. Marot et al. (2012) developed a new energy analysis of tests, linking the erosion rate to the power expended by fluid flow and the eroded clay

✉ Feng-shou ZHANG, fengshou.zhang@tongji.edu.cn

 Tuo WANG, <https://orcid.org/0000-0001-6884-2763>

Feng-shou ZHANG, <https://orcid.org/0000-0002-4998-6259>

Pei WANG, <https://orcid.org/0000-0003-3835-2477>

Received Apr. 4, 2022; Revision accepted Sept. 26, 2022;  
Crosschecked Nov. 28, 2022; Online first Jan. 23, 2023

© Zhejiang University Press 2023

mass to the energy dissipation. Rochim et al. (2017) experimentally investigated the effects of hydraulic loading history on the suffusion susceptibility of cohesionless soils.

In addition to internal factors, a large number of studies have been conducted focusing on external ones (Luo et al., 2013; Ke and Takahashi, 2015). Moffat and Fannin (2011) proposed, by erosion testing under  $K_0$  stress (which limits the lateral displacement of the sample and applies vertical pressure) conditions, the concept of hydromechanical pathways in stress-gradient space to describe the response of internal erosion to seepage flow. By performing stress-controlled erosion experiments, Chen et al. (2016) revealed that granular soils changed from the initial dilation to compaction after a significant loss of fine particles. Chang and Zhang (2013) investigated critical hydraulic gradients in the suffusion process by gradually increasing the hydraulic gradient, from which three critical gradients were defined: initiation, skeleton-deformation, and failure hydraulic gradients.

Despite these advances, a better understanding of the evolution process of fine particle migration at the pore scale and the interaction mechanism of coarse and fine particles is still needed. The selection mechanism of erosion channels under multiple outlets remains unclear. To this end, we develop a transparent apparatus and conduct experiments to investigate the suffusion process. To investigate the variation of pore scale in more detail and to conduct more parametric studies, a numerical model that is similar to the experimental one is created for reproducing the suffusion process in a sand layer with gap-graded grains, and three fluid outlets are designed to study the suffusion pattern under multiple outlets. This model can be used to reveal the migration process of fines in a coarse particle matrix and the formation process of the erosion channel.

The rest of this paper is organized as follows. Section 2 describes the physical experiments including model setup, testing material, testing procedure, and results and analysis. Section 3 introduces an experiment-based numerical simulation, which includes dynamic fluid mesh, governing equations, calculation of hydro-mechanical forces on the particles, coupling procedures, numerical model setup, simulation process and results, and experiment and simulation comparison. Section 4 presents parametric analysis

based on simulation. Finally, a summary is given in Section 5.

## 2 Laboratory experiments

Fig. 1 illustrates the suffusion process in a gap-graded sand layer under a hydraulic gradient. It is based on suffusion experiments and numerical simulation (Chang and Zhang, 2013; Cheng et al., 2018; Zhang et al., 2022). Fines move in the direction of the hydraulic gradient through pores formed by coarse particles under a drag force while the coarse particles only move slightly because they are subjected to greater resistance (friction and contact forces between particles). In the process, some fines are clogged and reaccumulated in pores or around coarse particles.

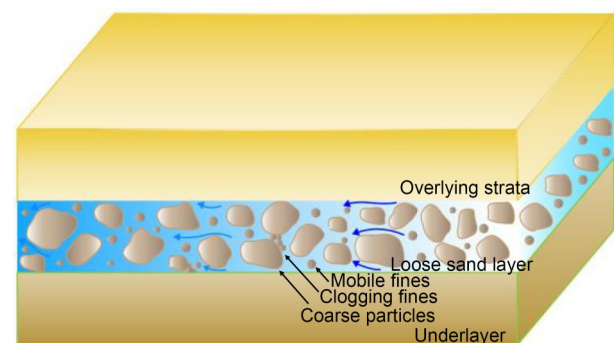


**Fig. 1** Schematic diagram of suffusion in a gap-graded sand layer

### 2.1 Physical model setup

To reproduce the phenomenon shown in Fig. 1, we designed a new physical model apparatus that allows fluid to flow into a specimen tank and sand particles to flow out from three outlets. Fig. 2a is a schematic diagram of the experimental apparatus which consists of a specimen tank, a camera, a water head control device, and a sewage collection device. The head control device includes a water supply tank and an overflow tank. The water supply tank sends water into the overflow tank. The overflow tank keeps the water surface stable during the experiments. Fig. 2b is a zoom-in view of the specimen tank. The tank is 100 mm long, 50 mm wide, and 15 mm deep. Some glass beads with a diameter of 4 mm are placed inside the tank to disperse water. A Cannon EOM M6 camera with a resolution of 2656×1992 pixels is mounted

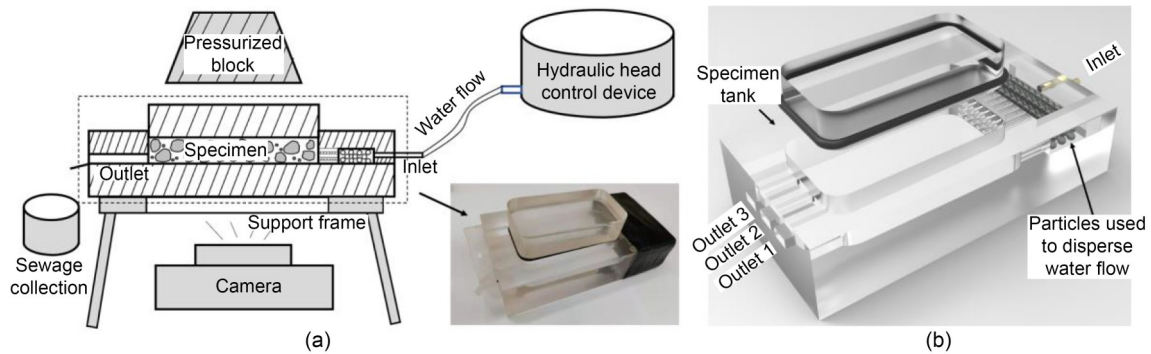


**Fig. 2** Schematic diagram of the experimental apparatus for investigating suffusion (a) and zoom-in view of the specimen tank (b)

150 mm below the specimen tank and provides high-resolution photographs recording the suffusion process at nine frames per second. A pressurized block is placed on the specimen tank to apply the  $K_0$  pressure on the sand sample. A sealing rubber is arranged around the top cover to prevent water from overflowing from the tank during the experiment. According to our measurement, when a 0.25-kg weight is applied to the top of the seal cap, the cap can overcome friction and begin to move. In this study, when applying  $K_0$  pressure, an additional 0.25-kg weight is applied to ensure accurate pressure. A water pressure control is connected to the inlet of the specimen tank and is used to supply a constant water head. According to similar experiments (Chang, 2012), based on the measured outflow velocity, the calculated head loss within the tubes is generally within 2% of the applied hydraulic head, and can be neglected. A beaker is placed under the outlets to collect the eroded sand. During the experiment, a new beaker is replaced every 5 s.

## 2.2 Testing material

In this study, the evolution process of suffusion is studied using gap-graded specimens. The advantages of using gap-graded specimens include: accelerating the suffusion process due to the internal instability of the gap-graded samples, facilitating the photographic recording of the process, and simplifying the analysis process by avoiding interference from medium-sized particles.

The gap-graded specimens consist of two types of particles. The coarse particles are glass beads with  $d_a$  of 6.25 mm and the small particles are silica sand with  $d_a$  of 0.75 mm, where  $d_a$  is the mean particle diameter. The particle size distribution is plotted in Fig. 3. According to the filter rules developed by Kenney

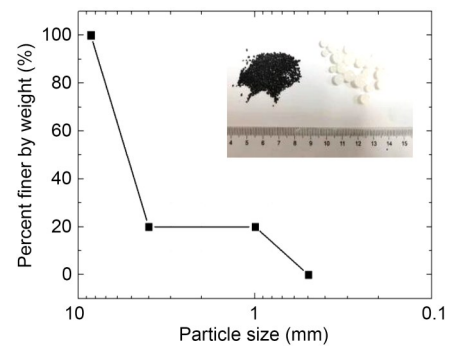


**Fig. 3** Particle size distribution of the testing material

and Lau (1985), the sample is internally unstable. To better distinguish between the two particle groups in the experiment, the coarse particles are colored white and the small particles are colored black. Other physical properties are listed in Table 1. The fines content (FC) in the experiments is set to 20% to reproduce the migration process of fines in the matrix formed by the coarse particles. The sample is soaked in water for 24 h to ensure saturation. Before the test, the sample is placed in the instrument. To prevent desaturation, testing is begun immediately.

**Table 1** Physical properties of the testing material

Property	Value
Dry density of fines, $\rho$ (g/cm <sup>3</sup> )	1.92
Specific gravity of fines, $G_{fs}$	2.65
Relative packing density (%)	70
Fines content, FC (%)	20
Diameter of fines (mm)	0.5–1.0
Specific gravity of coarse particles, $G_{cs}$	2.65
Diameter of coarse particles (mm)	4.0–8.5
Coefficient of friction of fines	0.60
Coefficient of friction of coarse particles	0.56

### 2.3 Testing procedure

In the experiment, the effect of the hydraulic gradient is examined by three tests with different hydraulic gradients. The main purpose of this experiment is to reproduce the evolution process of suffusion caused by water flowing into a gap-graded specimen. The experimental procedure is as follows:

- (1) Mix the coarse particles and fines and ensure that the FC is 20% and the sample is saturated.
- (2) Install the instruments, connect the hydraulic head control device to the specimen tank, and place the camera and beaker.
- (3) Place the specimen and place the pressurized block on the cover of the specimen tank to reach 20-kPa  $K_0$  pressure, and ensure that the specimen is compacted.
- (4) Adjust the hydraulic head to the desired height (2, 4, and 8 kPa) and turn on the switch to allow water to flow into the specimen tank.
- (5) Record the experimental process and collect the eroded particles in the beaker.
- (6) Dry the suffusion particles and weigh them.

### 2.4 Experimental results and analysis

The evolution processes of suffusion under 2, 4, and 8 hydraulic gradients are shown in Fig. 4, and the obvious erosion zones are marked in rectangle. As shown in Fig. 4, the specimen is homogeneous before the fluid flows into the specimen tank. However, after the suffusion process starts, some particles are lost from the outlets and some erosion zones in which fines are lost appear inside the specimen. The area and the number of erosion zones increase with time. The erosion areas show obvious localization characteristics. In some zones, the loss of fine particles is severe; in other zones, however, suffusion is not as pronounced. In the initial stage, the erosion zone is small. Subsequently, the area gradually expands. At the end of the test, the area of erosion zones is stabilized. In addition, as the hydraulic gradient increases, so do the area and number of erosion zones.

The erosion curve in Fig. 5 shows the same results. The final erosion weight increases with the increment of the hydraulic gradient. Under the lower hydraulic gradients (2 and 4), most of the particles are lost in the initial stage and the suffusion rate becomes zero after 5 s. Under the hydraulic gradient of 8, the suffusion rate decreases gradually over time but the

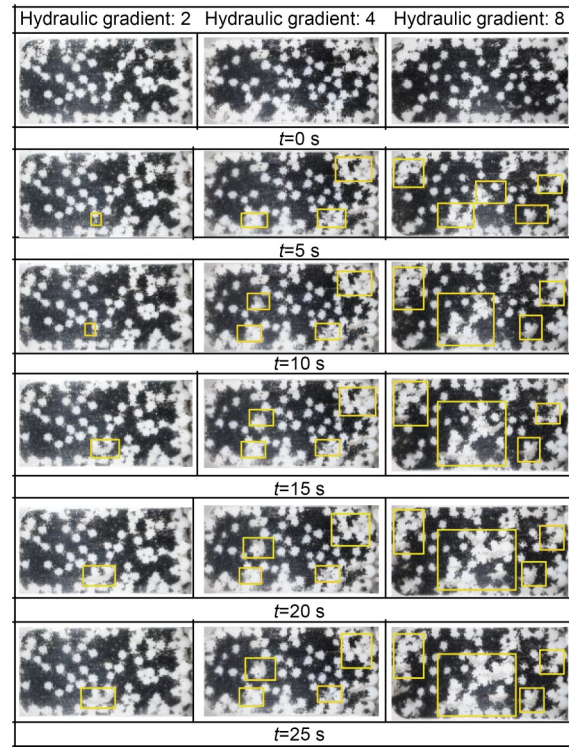


Fig. 4 Evolution process of suffusion under hydraulic gradients of 2, 4, and 8

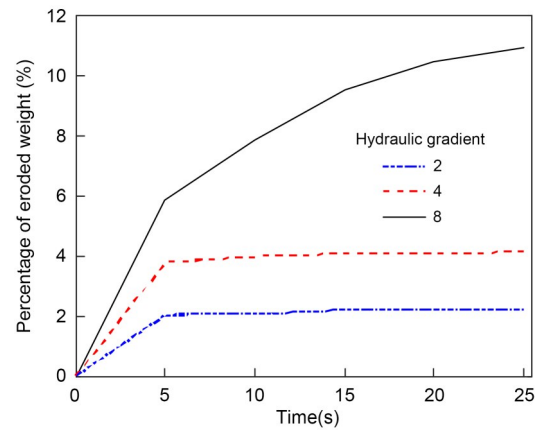


Fig. 5 Percentage of eroded weight (the suffusion mass divided by the total sample mass) under different hydraulic gradients

rate of reduction is slower. With the increase of hydraulic gradient, the amount of internal erosion increases and the process of internal erosion increases. When the hydraulic gradient is 8, during the test time, the internal erosion lasts for a longer time and does not enter a stable stage. Therefore, the curve of the hydraulic gradient of 8 is different from the others.



### 3 Numerical simulation

To further investigate the suffusion mechanism, especially at the pore scale, we establish a discrete element method (DEM) model based on the experimental setup. All numerical models in this study are performed using a dynamic fluid mesh (DFM) algorithm developed based on the particle flow code (PFC) (Itasca Consulting Group Inc., 2015). To capture changes in pores dynamically formed by particles, Zhang et al. (2020) developed a DFM method. Reference should be made to the electronic supplementary materials (ESM) for a detailed description of the DFM's mesh generation, governing equations, and drag force model.

The flowchart of the coupling procedure is presented in Fig. 6. A DEM model of gap-graded soil is generated first. Subsequently, a DFM is created with a Python script based on a coarse center. The  $k$ -dimensional tree (KD-tree) algorithm (Silpa-Anan and Hartley, 2008) is used to locate fine particles and then calculate the permeability of each pore through the Konzeny-Carman equation. A Laplace equation is solved to obtain the pressure gradients in each grid and flow velocity is solved according to Darcy's law. After that, the drag forces on coarse and fine particles are applied. In the DEM software, the position and contact force of the particles are updated. The process is repeated until the calculation is complete.

#### 3.1 Numerical model setup

To reproduce the phenomenon in the experiment, a cuboid assembly of gap-graded particles is generated by the coupled DEM-DFM (Fig. 7). In the model, we focus on the horizontal migration of fines. The length, width, and height of the sample are 10, 5, and 1 cm, respectively. The computational region is enclosed by six walls. The front wall has three rectangular outlets for fines to pass through and to block coarse particles. The length of the outlets is 1.0 cm and the width is 0.5 cm. Forces are applied onto the top wall and subjected to a servo-controlled mechanism for a constant effective confining stress (20 kPa in the base case simulation). The other walls are fixed. The hydraulic head is applied to the back wall (80 cm in the base case), and zero at the outlets. No flux is allowed on the other walls, so the fluid flow is only in the horizontal direction. To ensure specimen uniformity, gravity and buoyancy are not considered in the model.

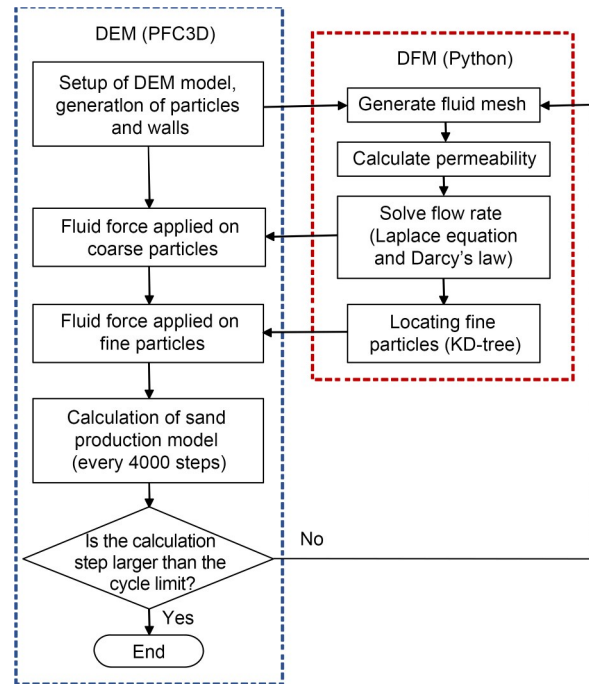


Fig. 6 Flowchart of the DEM-DFM coupling process

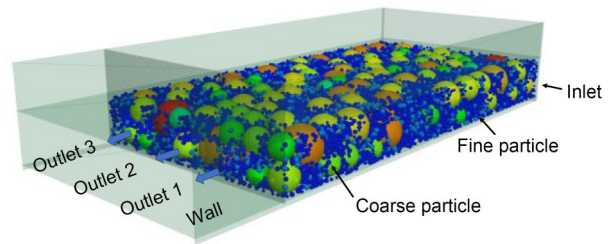


Fig. 7 Experiment-based numerical model setup for understanding suffusion

The gap-graded samples consist of two groups of particles of large and small sizes. The radius of the coarse particles ranges from 4.18 to 8.50 mm, and the radius of fines ranges from 0.468 to 1.036 mm. The diameter of the coarse particles is on average 8 times greater than that of the fine particles and both of them follow a uniform distribution. In benchmarking, suffusion is studied using a sample with an FC of 20% (fines accounting for 20% of the total weight). In the parametric analysis, two models with FC=10% and 30% are added. The total numbers of particles in these models are 7959, 17953, and 30823, respectively. The number of coarse particles in all specimens is 159. In this work we use the rolling resistance contact model to represent the contact relationship between particles (a detailed description is provided in the ESM), which dissipates energy during particle rotation (Zhang et al.,

2019). Many studies have been conducted to investigate the microscopic parameters (Nardelli et al., 2017; Wang et al., 2022b). Based on a previous study (Zhang et al., 2019), the normal-to-shear stiffness ratio is set to 2, and a friction coefficient of 0.6 is adopted. The input parameters are listed in Table 2.

**Table 2** Input parameters in the numerical model

Model parameter	Value
Normal stiffness of coarse particles (N/m)	$8.0 \times 10^5$
Normal stiffness of fine particles (N/m)	$1.0 \times 10^5$
Average radius of coarse particles (m)	$3.2 \times 10^{-3}$
Average radius of fine particles (m)	$4.0 \times 10^{-4}$
Normal-to-shear stiffness ratio	2.0
Coefficient of friction	0.6
Rolling resistance coefficient	0.1
Particle density ( $\text{kg/m}^3$ )	2650
Normal stiffness of wall (N/m)	$1.0 \times 10^5$
Shear stiffness of wall (N/m)	$5.0 \times 10^3$

### 3.2 Simulation process and results

In this study, the simulation process can be divided into three stages: specimen generation, flow field activation, and suffusion simulation. First, some uniform particles are generated within the simulation area and 159 particles are randomly selected for grouping. The remaining particles are grouped into another group. Subsequently, the particle size of the 159 particles is increased, while the size of the remaining particles is

decreased until the average particle size ratio of the two groups is 8. The specimen volume remains unchanged during the process. The ratio of average unbalance of the model is reduced to 0.01 in order to decrease the energy of the specimen. Excess of fine particles is randomly removed according to the targets of FC (10%, 20%, and 30%). The confining stress is applied to the top wall and the other walls are fixed to consolidate the sample. The consolidation process is completed after a total of 100000-time steps, approximately reaching the force equilibrium. The front wall is then replaced by a wall with outlets.

In the second stage, a tetrahedral fluid mesh is built according to the centers of the coarse particles and the contact points between the coarse particles and the walls (Fig. 8a). Thereafter, a water pressure of 8 kPa is applied at the inlet of the model and the pore pressure is solved (Fig. 8b), and the flow force is applied to the coarse particles. Based on Darcy's law, the flow field is calculated (Fig. 8c) and the drag force is applied to the fine particles. To represent the migration of fines in the sample, porosity is also solved and shown in Fig. 8d.

After the flow field is activated, erosion starts. The suffusion curve is shown in Fig. 9a. The eroded weight increases rapidly in the first few seconds, and then the erosion rate slows down gradually with the simulation time. At the initial time, the erosion rate is fast. This is because the initially eroded particles are located near the outlets. When seepage forces are applied to the particles, these particles quickly disappear.

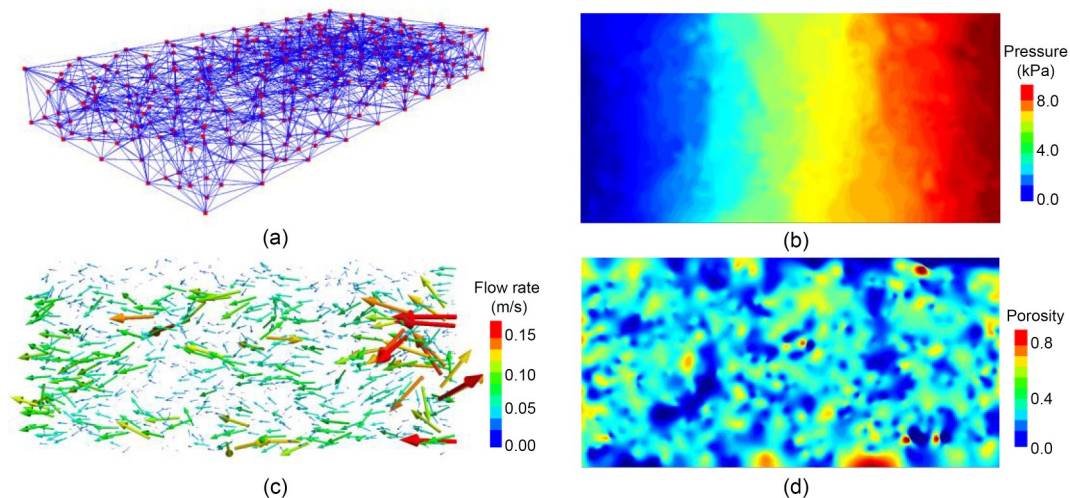


**Fig. 8** Initial states of the numerical model with 20% FC: (a) initial mesh; (b) pore pressure; (c) flow velocity in each grid; (d) initial porosity

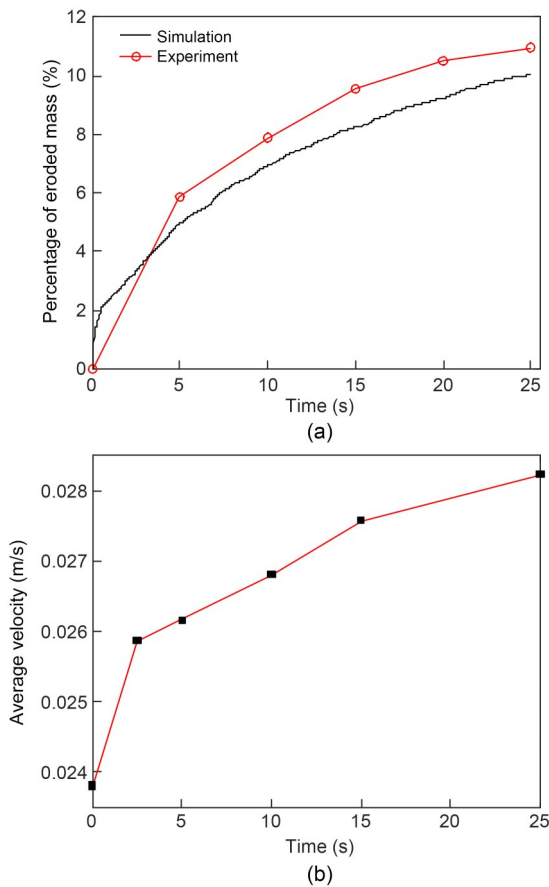


**Fig. 9** Comparison of suffusion curves between the experiment and numerical simulation with 20% FC (a) and evolution of average flow velocity of pores during suffusion (b)

Subsequently, particles further away from the outlets are lost more gradually. Due to the barrier between the particles, particles far from the outlet are not so easily lost, so the erosion rate gradually slows down. The evolution of average flow velocity of the grids is essentially synchronized with the evolution of erosion rate (Fig. 9b). In the initial stage, the average flow velocity increases rapidly as the erosion weight increases. Subsequently, as the erosion rate gradually decreases, the average flow velocity increases slowly.

Fig. 10 shows the changes of the assembly of the numerical model during the suffusion process. Before the erosion begins, fine particles in the specimen are evenly distributed. After the fluid pressure is applied, the fines move to the outlets following the pressure reduction direction. The particles near the outlets are quickly lost, and at 5 s, a significant erosion is seen at the outlets. At 10 s, the porosity and the erosion zone near the outlets continue to increase. At 15 s, the

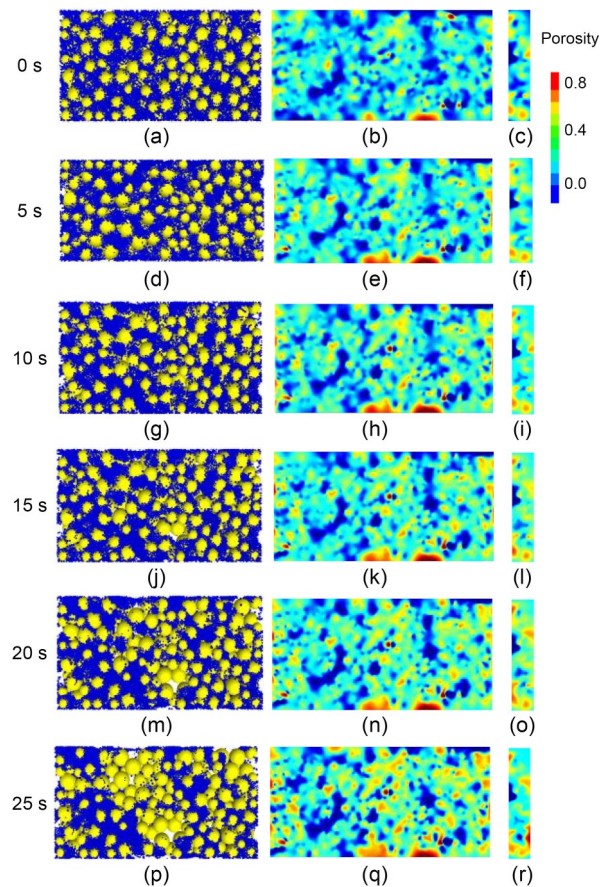


**Fig. 10** Evolution process of suffusion and the corresponding changes in porosity, top view of sample (a, d, g, j, m, and p), and horizontal (b, e, h, k, n, and q) and cross sections (c, f, i, l, o, and r) of porosity

erosion inside the specimen can be clearly seen. Subsequently, the erosion zone in the specimen expands, and the porosity of the severely eroded area gradually increases. At 25 s, large areas of erosion are formed, in which coarse particles are completely exposed. The fines show a pronounced aggregation phenomenon and accumulate in some pores made of coarse particles. The entire model forms apparent erosion and blocking zones.

From the view of the contact force chain, the same results are obtained. As shown in Fig. 11, in the initial stage, there are only a few contacts between coarse particles and fines. As the erosion goes on, the contacts between coarse particles and fines and between the fines increase. After 5 s, the distribution of force chains is obviously localized and is consistent with aggregation of fines.

As erosion becomes localized, flow velocity is also localized. Fig. 12 shows the profiles of the model



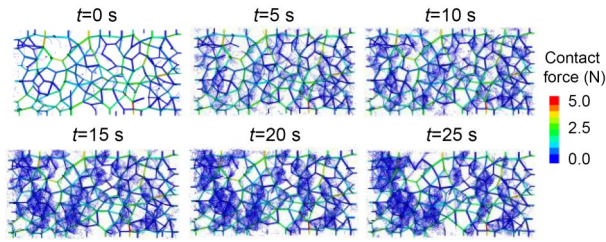


**Fig. 11** Variation of force chains during suffusion in the model with 20% FC

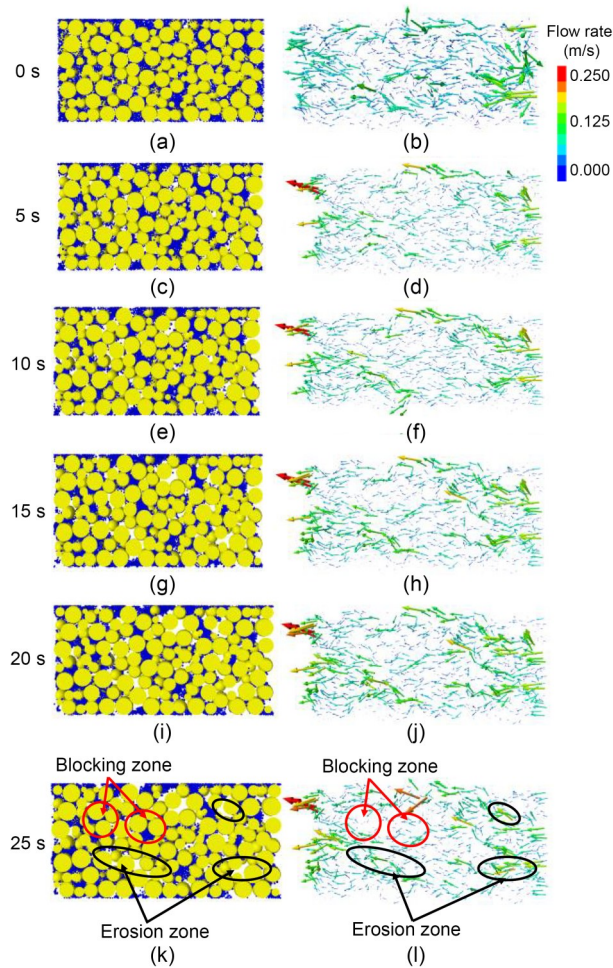


**Fig. 12** Evolution of erosion zone (a, c, e, g, i, and k) and flow velocity (b, d, f, h, j, and l)

and the flow velocity synchronized with the suffusion. In the profile, erosion and blocking zones can be clearly seen. The flow velocity in the erosion zone is faster than that in the blocked zone. In addition, compared with the initial stage, the inhomogeneity of flow velocity increases in the sample.

To investigate the erosion of each section, the specimen is evenly divided into five sections from

outlets to the inlet boundary (the first section is near the outlets). As shown in Fig. 13a, the 5th section has the largest reduction in fines weight; however, in the final stage of the simulation, the erosion weight remains approximately the same. The weight loss of the 4th section is lower than that of the 3rd section. This is because more erosion zones are in the 3rd section of the specimen. Some fines from the 5th section are blocked in the 4th section and cannot enter the 3rd section. The weight of the 3rd section first increases and then decreases, remaining roughly unchanged throughout the simulation. This is because the amount of fine particles lost is roughly equal to the amount moved in. The weight of the 1st section increases because there are a large number of fines that are clogged in the area, many more than those eroded.

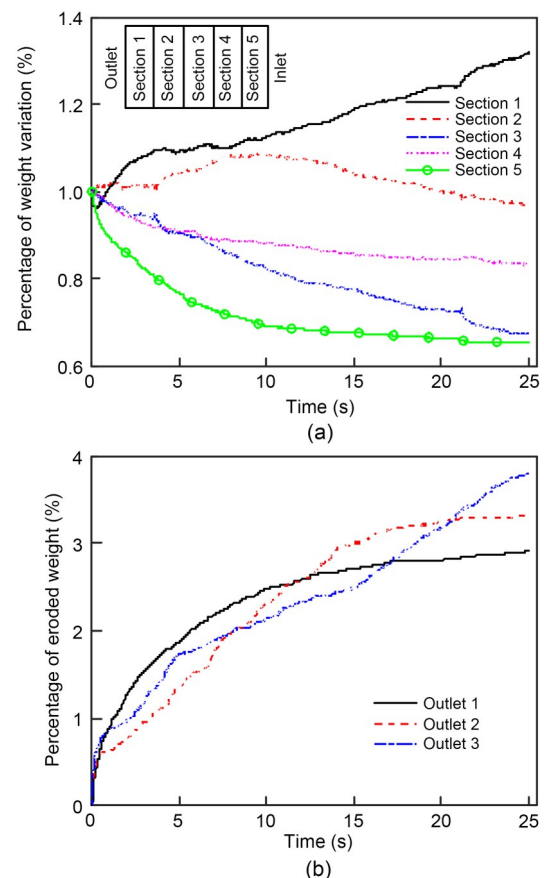


**Fig. 13** Percentage of weight variation in each section (a) and percentage of eroded weight in each outlet (b) during suffusion

The eroded weight at each outlet is shown in Fig. 13b. In the initial stage, fines are poured out near the outlets and the erosion rates from the three outlets



are approximately equal. Subsequently, the erosion rates decrease, consistent with the erosion curve shown in Fig. 9. The erosion rate curve for outlet 1 is smoother throughout the simulation, but the erosion rates at outlets 2 and 3 increase continuously. This may be due to the fact that the erosion channel connecting outlet 1 is more open. In the final stage, the erosion rates at outlets 1 and 2 become approximately zero, while outlet 3 still shows continued particle loss. The reason could be that the erosion rate decreases and then increases in the curve for outlet 3, which indicates that erosion may occur in phases.

### 3.3 Comparison of experimental and simulation results

To verify the reliability of the coupled numerical simulation, comparisons of the evolution process and suffusion curves are presented in Figs. 14 and 9, respectively.

The variation of erosion rate and the trend of the suffusion curve are similar to those of the experiment. The percentages of eroded weight in the experiment and numerical simulation are 10.96% and 10.04%, respectively. The difference may be due to the non-uniformity of the experimental and simulated specimens.

As shown in Fig. 14, compared with the experiment, the same erosion process is also presented in the simulation. The erosion zone also gradually expands in the simulation. Moreover, at 25 s, suffusion and blocking zones also appear in the simulation, similar to the experimental results. The results show that the coupled DEM-DFM model can be used to investigate the suffusion in gap-graded soil.

## 4 Parametric study of numerical simulation

### 4.1 Effect of the hydraulic gradient

To investigate the effect of the hydraulic gradient, we set up three models with different hydraulic heads at the inlet (80, 140, and 200 cm) while maintaining a  $K_0$  pressure of 20 kPa and the FC of 20%. A positive correlation between the pressure gradient and the erosion weight is observed, as shown in Fig. 15. In the initial stage, the eroded weight increases rapidly. Subsequently, the erosion weight levels off and the erosion rates also gradually decrease over time.

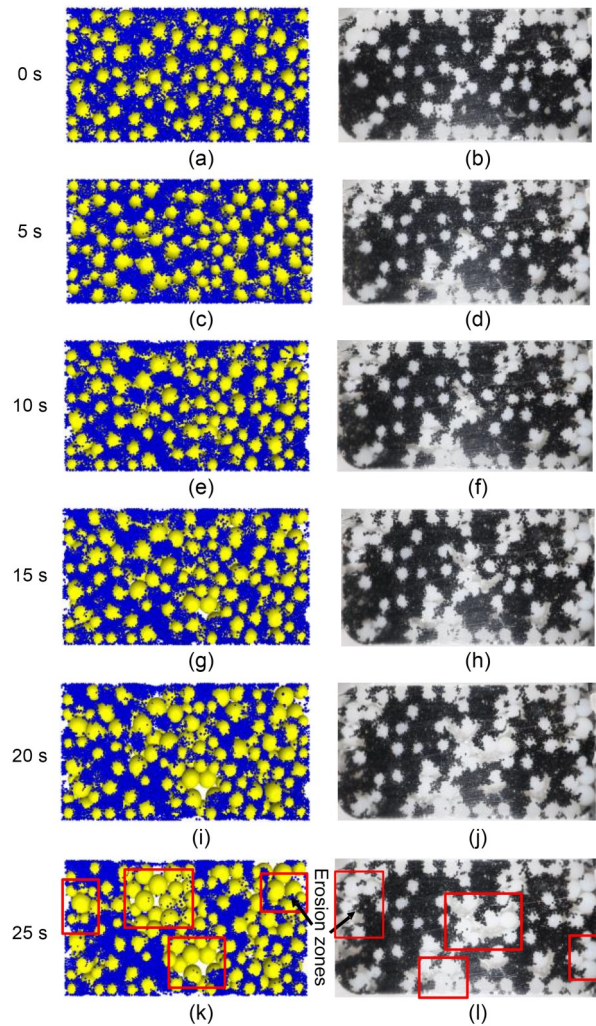


Fig. 14 Comparison of the evolution process between the numerical simulation (a, c, e, g, i, and k) and the experiment (b, d, f, h, j, and l)

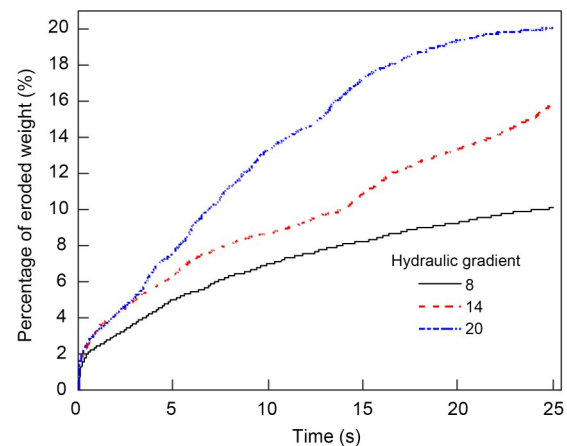


Fig. 15 Percentage of eroded weight under different hydraulic gradients

#### 4.2 Effect of fines content

Fig. 16 shows the numerical results for cases with different FCs (10%, 20%, and 30%). The variation of the percentage of eroded weight during suffusion is shown in Fig. 16a. The model with an FC of 10% has the most fines loss. The fines losses with a content of 20% and 30% are roughly the same. However, as shown in Fig. 16b, the eroded weight of the fines increases with the increment of the FC. The results also consist with the study of Liu et al. (2020). This may be because fine particles have higher mobility in models with lower FC and the flow velocity under the same hydraulic gradient is faster due to higher porosity. Therefore, the model with the lowest FC has the highest percentage of eroded weight. However, lower FC leads to lower eroded weight.

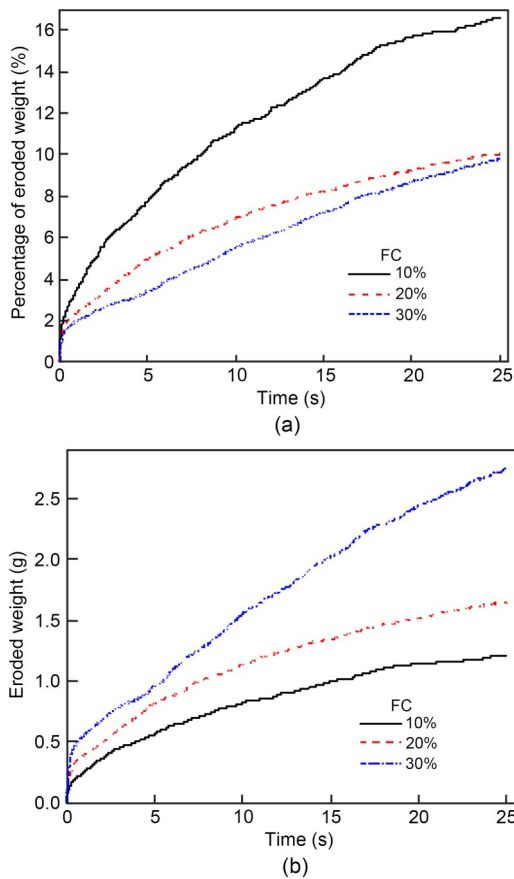


Fig. 16 Variation of percentage of eroded weight (a) and variation of eroded weight (b) during suffusion

#### 4.3 Response to $K_0$ pressure

To explore the effect of  $K_0$  pressure in fines migration, we perform simulations with an FC of 10%

under three different  $K_0$  pressures. The results are shown in Fig. 17, where the eroded weight increases as the  $K_0$  pressure decreases. The erosion rates are the same under different  $K_0$  pressures in the initial stage. Afterwards, as the loss of fine particles develops, the difference in eroded weight under different  $K_0$  pressures gradually becomes apparent. The reason is that the movement of the fine particles near the outlets is less affected by the confining stress. Near the outlet, the particles are not supported by the wall in the outlet direction, and confining pressures do not completely limit the movement of these particles, so they are easy to lose under the drag force. In addition, the flow velocity is faster at the outlets, resulting in a rapid initial loss rate, which leads to the loss of particles near the outlets in a very short time. However, for particles far from the outlets, lower confining stress leads to less friction between particles, which facilitates particle movement.

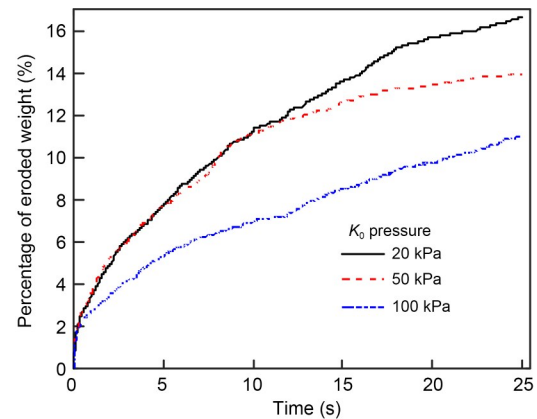


Fig. 17 Percentage of eroded weight under different  $K_0$  pressures

## 5 Conclusions

In this study, we propose a new method to quantify the suffusion process in gap-graded soils through a series of experiments and numerical simulations using the coupled DEM-DFM. First, physical experiments are carried out to reproduce suffusion through a horizontal apparatus with three outlets, and the effect of the hydraulic gradient is investigated. Subsequently, based on the physical model test results, we develop a new DEM numerical model to reveal the erosion mechanism at the pore scale and to further study the influencing factors. The simulation results are generally

consistent with the experimental data. The following conclusions can be drawn from this work:

(1) As erosion progresses, erosion zones are formed inside the specimen and gradually expand. From the force chain analysis, fines gradually accumulate in the pores formed by coarse particles under the action of water flow and are blocked by the coarse particles.

(2) As erosion and blocking zones are formed, flow velocities are also localized. In the erosion zone, the porosity increases, and the flow velocity is generally fast. However, in the blocking zone, the flow velocity is slow.

(3) From the evolution of erosion and flow velocity, it is concluded that many particles are transported away by the water flow, and the flow velocity rises rapidly in the pores in the initial stage of erosion. Subsequently, the erosion rate decreases gradually, and the fluid velocity eventually reaches a steady state.

(4) Parametric analysis shows a positive correlation between the final eroded weight and the hydraulic gradient. The eroded weight decreases as the  $K_0$  pressure increases. As the FC increases, the eroded weight increases. However, in the model with a lower FC, a larger fines fraction is lost.

In this study, in order to clearly observe the migration process of fine particles, the model has a shorter height in the vertical direction, which is deficient in stress uniformity. However, during the experiment and simulation, the skeleton of coarse particles is mainly stressed and the coarse particles do not move much during the process, so the stress distribution should have little influence on the model. In some experiments, a fluid channel is often formed between the particles and the sample and the water flow is faster. This is not well reproduced in the simulation, which may lead to a lower amount of eroded mass in the simulation. In addition, according to previous studies (Shire and O'Sullivan, 2013; Ahmadi et al., 2020), relative density will influence the internal stability of a gap-graded sample; however, according to some suffusion studies (Cheng et al., 2018; Huang et al., 2021), the overall trend will not change as the relative density varies.

## Acknowledgments

This work is supported by the National Key Research and Development Program of China (No. 2020YFC1808102) and the National Natural Science Foundation of China (Nos. 42077247 and 42002271).

## Author contributions

Feng-shou ZHANG and Tuo WANG designed the research. Tuo WANG processed the corresponding data. Tuo WANG wrote the first draft of the manuscript. Pei WANG helped to organize the manuscript. Feng-shou ZHANG revised and edited the final version.

## Conflict of interest

Tuo WANG, Feng-shou ZHANG, and Pei WANG declare that they have no conflict of interest.

## References

- Ahmadi M, Shire T, Mehdizadeh A, et al., 2020. DEM modeling to assess internal stability of gap-graded assemblies of spherical particles under various relative densities, fine contents and gap ratios. *Computers and Geotechnics*, 126:103710.  
<https://doi.org/10.1016/j.compgeo.2020.103710>
- Bendahmane F, Marot D, Alexis A, 2008. Experimental parametric study of suffusion and backward erosion. *Journal of Geotechnical and Geoenvironmental Engineering*, 134(1):57-67.  
[https://doi.org/10.1061/\(asce\)1090-0241\(2008\)134:1\(57\)](https://doi.org/10.1061/(asce)1090-0241(2008)134:1(57))
- Chang DS, 2012. Internal Erosion and Overtopping Erosion of Earth Dams and Landslide Dams. PhD Thesis, Hong Kong University of Science and Technology, Hong Kong, China.
- Chang DS, Zhang LM, 2011. A stress-controlled erosion apparatus for studying internal erosion in soils. *Geotechnical Testing Journal*, 34(6):GTJ103889.  
<https://doi.org/10.1520/GTJ103889>
- Chang DS, Zhang LM, 2013. Critical hydraulic gradients of internal erosion under complex stress states. *Journal of Geotechnical and Geoenvironmental Engineering*, 139(9): 1454-1467.  
[https://doi.org/10.1061/\(asce\)gt.1943-5606.0000871](https://doi.org/10.1061/(asce)gt.1943-5606.0000871)
- Chen C, Zhang LM, Chang DS, 2016. Stress-strain behavior of granular soils subjected to internal erosion. *Journal of Geotechnical and Geoenvironmental Engineering*, 142(12): 06016014.  
[https://doi.org/10.1061/\(asce\)gt.1943-5606.0001561](https://doi.org/10.1061/(asce)gt.1943-5606.0001561)
- Cheng K, Wang Y, Yang Q, 2018. A semi-resolved CFD-DEM model for seepage-induced fine particle migration in gap-graded soils. *Computers and Geotechnics*, 100:30-51.  
<https://doi.org/10.1016/j.compgeo.2018.04.004>
- Golay F, Bonelli S, 2011. Numerical modeling of suffusion as an interfacial erosion process. *European Journal of Environmental and Civil Engineering*, 15(8):1225-1241.  
<https://doi.org/10.1080/19648189.2011.9714850>
- Hu Z, Zhang YD, Yang ZX, 2019. Suffusion-induced deformation and microstructural change of granular soils: a coupled CFD-DEM study. *Acta Geotechnica*, 14(3):795-814.  
<https://doi.org/10.1007/s11440-019-00789-8>
- Huang Z, Bai YC, Xu HJ, et al., 2021. A theoretical model to predict suffusion-induced particle movement in cohesionless soil under seepage flow. *European Journal of Soil Science*, 72(3):1395-1409.



- <https://doi.org/10.1111/ejss.13062>
- Hunter RP, Bowman ET, 2018. Visualisation of seepage-induced suffusion and suffosion within internally erodible granular media. *Géotechnique*, 68(10):918-930. <https://doi.org/10.1680/jgeot.17.P.161>
- Itasca Consulting Group Inc., 2015. PFC3D (Particle Flow Code in 3 Dimensions), Version 5.0. Itasca Consulting Group Inc., Minneapolis, USA.
- Ji SM, Ge JQ, Tan DP, 2017. Wall contact effects of particle-wall collision process in a two-phase particle fluid. *Journal of Zhejiang University-SCIENCE A (Applied Physics & Engineering)*, 18(12):958-973. <https://doi.org/10.1631/jzus.A1700039>
- Jin Z, Lu Z, Yang Y, 2021. Numerical analysis of column collapse by smoothed particle hydrodynamics with an advanced critical state-based model. *Journal of Zhejiang University-SCIENCE A (Applied Physics & Engineering)*, 22(11):882-893. <https://doi.org/10.1631/jzus.A2000598>
- Ke L, Takahashi A, 2014. Experimental investigations on suffusion characteristics and its mechanical consequences on saturated cohesionless soil. *Soils and Foundations*, 54(4):713-730. <https://doi.org/10.1016/j.sandf.2014.06.024>
- Ke L, Takahashi A, 2015. Drained monotonic responses of suffusional cohesionless soils. *Journal of Geotechnical and Geoenvironmental Engineering*, 141(8):04015033. [https://doi.org/10.1061/\(ASCE\)GT.1943-5606.0001327](https://doi.org/10.1061/(ASCE)GT.1943-5606.0001327)
- Kenney TC, Lau D, 1985. Internal stability of granular filters. *Canadian Geotechnical Journal*, 22(2):215-225. <https://doi.org/10.1139/t85-029>
- Liu Q, Zhao B, Santamarina JC, 2019. Particle migration and clogging in porous media: a convergent flow microfluidics study. *Journal of Geophysical Research: Solid Earth*, 124(9):9495-9504. <https://doi.org/10.1029/2019JB017813>
- Liu YJ, Wang LZ, Hong Y, et al., 2020. A coupled CFD-DEM investigation of suffusion of gap graded soil: coupling effect of confining pressure and fines content. *International Journal for Numerical and Analytical Methods in Geomechanics*, 44(18):2473-2500. <https://doi.org/10.1002/nag.3151>
- Luo YL, Qiao L, Liu XX, et al., 2013. Hydro-mechanical experiments on suffusion under long-term large hydraulic heads. *Natural Hazards*, 65(3):1361-1377. <https://doi.org/10.1007/s11069-012-0415-y>
- Marot D, Le VD, Garnier J, et al., 2012. Study of scale effect in an internal erosion mechanism: centrifuge model and energy analysis. *European Journal of Environmental and Civil Engineering*, 16(1):1-19. <https://doi.org/10.1080/19648189.2012.667203>
- Moffat R, Fannin RJ, 2011. A hydromechanical relation governing internal stability of cohesionless soil. *Canadian Geotechnical Journal*, 48(3):413-424. <https://doi.org/10.1139/T10-070>
- Moffat R, Fannin RJ, Garner SJ, 2011. Spatial and temporal progression of internal erosion in cohesionless soil. *Canadian Geotechnical Journal*, 48(3):399-412. <https://doi.org/10.1139/T10-071>
- Nardelli V, Coop MR, Andrade JE, et al., 2017. An experimental investigation of the micromechanics of Eglin sand. *Powder Technology*, 312:166-174. <https://doi.org/10.1016/j.powtec.2017.02.009>
- Rochim A, Marot D, Sibille L, et al., 2017. Effects of hydraulic loading history on suffusion susceptibility of cohesionless soils. *Journal of Geotechnical and Geoenvironmental Engineering*, 143(7):04017025. [https://doi.org/10.1061/\(asce\)gt.1943-5606.0001673](https://doi.org/10.1061/(asce)gt.1943-5606.0001673)
- Shire T, O'Sullivan C, 2013. Micromechanical assessment of an internal stability criterion. *Acta Geotechnica*, 8(1):81-90. <https://doi.org/10.1007/s11440-012-0176-5>
- Shire T, O'Sullivan C, Hanley KJ, et al., 2014. Fabric and effective stress distribution in internally unstable soils. *Journal of Geotechnical and Geoenvironmental Engineering*, 140(12):04014072. [https://doi.org/10.1061/\(ASCE\)GT.1943-5606.0001184](https://doi.org/10.1061/(ASCE)GT.1943-5606.0001184)
- Silpa-Anan C, Hartley R, 2008. Optimised KD-trees for fast image descriptor matching. *IEEE Conference on Computer Vision & Pattern Recognition*, p.1-8. <https://doi.org/10.1109/CVPR.2008.4587638>
- Tang Y, Yao XY, Chen YN, et al., 2020. Experiment research on physical clogging mechanism in the porous media and its impact on permeability. *Granular Matter*, 22(2):37. <https://doi.org/10.1007/s10035-020-1001-8>
- Tao R, Yang MM, Li SQ, 2018. Filtration of micro-particles within multi-fiber arrays by adhesive DEM-CFD simulation. *Journal of Zhejiang University-SCIENCE A (Applied Physics & Engineering)*, 19(1):34-44. <https://doi.org/10.1631/jzus.A1700156>
- Wan CF, Fell R, 2008. Assessing the potential of internal instability and suffusion in embankment dams and their foundations. *Journal of Geotechnical and Geoenvironmental Engineering*, 134(3):401-407. [https://doi.org/10.1061/\(asce\)1090-0241\(2008\)134:3\(401\)](https://doi.org/10.1061/(asce)1090-0241(2008)134:3(401))
- Wang P, Ge Y, Wang T, et al., 2022a. CFD-DEM modelling of suffusion in multi-layer soils with different fines contents and impermeable zones. *Journal of Zhejiang University-SCIENCE A (Applied Physics & Engineering)*, in press. <https://doi.org/10.1631/jzus.A2200108>
- Wang P, Yin ZY, Wang ZY, 2022b. Micromechanical investigation of particle-size effect of granular materials in biaxial test with the role of particle breakage. *Journal of Engineering Mechanics*, 148(1):04021133. [https://doi.org/10.1061/\(asce\)jem.1943-7889.0002039](https://doi.org/10.1061/(asce)jem.1943-7889.0002039)
- Wen MJ, Wang KH, Wu WB, et al., 2021. Dynamic response of bilayered saturated porous media based on fractional thermoelastic theory. *Journal of Zhejiang University-SCIENCE A (Applied Physics & Engineering)*, 22(12):992-1004. <https://doi.org/10.1631/jzus.A2100084>
- Yang J, Yin ZY, Laouafa F, et al., 2019. Analysis of suffusion in cohesionless soils with randomly distributed porosity and fines content. *Computers and Geotechnics*, 111:157-171. <https://doi.org/10.1016/j.compgeo.2019.03.011>
- Yin ZY, Jin YF, Zhang X, 2021. Large deformation analysis in

- geohazards and geotechnics. *Journal of Zhejiang University-SCIENCE A (Applied Physics & Engineering)*, 22(11): 851-855.  
<https://doi.org/10.1631/jzus.A21LDGG1>
- Zhang FS, Li ML, Peng M, et al., 2019. Three-dimensional DEM modeling of the stress-strain behavior for the gap-graded soils subjected to internal erosion. *Acta Geotechnica*, 14(2):487-503.  
<https://doi.org/10.1007/s11440-018-0655-4>
- Zhang FS, Wang T, Liu F, et al., 2020. Modeling of fluid-particle interaction by coupling the discrete element method with a dynamic fluid mesh: implications to suffusion in gap-graded soils. *Computers and Geotechnics*, 124:103617.  
<https://doi.org/10.1016/j.compgeo.2020.103617>
- Zhang FS, Wang T, Liu F, et al., 2022. Hydro-mechanical coupled analysis of near-wellbore fines migration from unconsolidated reservoirs. *Acta Geotechnica*, 17(8):3535-3551.  
<https://doi.org/10.1007/s11440-021-01396-2>

#### **Electronic supplementary materials**

Sections S1 and S2